Self-reanimating chaos in the bouncing-ball system

Zbigniew J. Kowalik, Marek Franaszek,* and Piotr Pierański
Institute of Molecular Physics, Polish Academy of Sciences, Smoluchowskiego 17/19, PL-60-179 Poznan, Poland
(Received 20 June 1986; revised manuscript received 15 April 1987)

The bouncing-ball problem was studied both experimentally and numerically. A qualitatively new behavior—so-called "self-reanimating" chaos—was found. In the experiment this behavior can be regarded as fully chaotic, but treated as regular motion (a cycle of large period) in the analytical approach.

I. INTRODUCTION

One of the simplest dynamical systems displaying a chaotic behavior is the bouncing-ball model.[1-4] This model was previously investigated by many authors in its original version or as the Fermi-Ulam problem.[2]

Usually, the dynamics of the bouncing ball is described by the dissipative standard map. However, in the experiment, where the ball is made to move on the vibrating surface, one can observe a particular kind of the ball motion. For small values of vibration amplitude, it takes the form of a periodically repeated series of decaying jumps, and for greater values (in the chaotic region) the irregular motion is randomly interrupted by such decaying sequences. The latter case, being the noise-induced chaotic motion, will be referred to as "self-reanimating chaos." These new kinds of motions can be found numerically using a more precise mapping, which takes into account the displacement of the vibrating surface.

We believe that the main mechanism underlying this chaotic effect is the existence of a trivial part of the attractor, which has continuous positive measure, in addition to a discrete part. Hereafter, the trivial attractor represents an immobility of the ball in relation to the vibrating surface. Thus the whole attractor corresponding to the self-reanimating chaos consists of the two topologically different parts: the first being purely chaotic (in experiment) and the second part being trivial. The properties of the chaotic part of the attractor such as the shape of trajectories in phase space or the integral dimension do not differ from those of the dissipative standard map, being a simplification of our model.

The behavior of the bouncing-ball system in the chaotic region (above the first period-doubling bifurcation limit) seems to be extremely complicated. Hitherto, we have been unable to conclude whether the self-reanimating chaos is a persisting or transitory phenomenon, especially when we have repeatedly observed the stabilization of the periodic motion. In such cases the above-mentioned effect should rather be referred to as the self-reanimating transient chaos.

Analytical studies of the extended map of the bouncing-ball show that in the absence of noise, the attractor corresponding to the experimental, self-reanimating behavior is a very long periodic cycle very sensitive to the external perturbations. Moreover, it can be shown that the unusual behavior of the bouncing-ball system is related to the properties of basin boundaries.[5] Namely, a fragment of the boundaries behaves like an attractor, i.e., trajectories initialized inside the basin can approach either the stable points from the interior of the basin or they can be attracted to some part of the basin boundaries. In the first case a stable cycle arises, while in the second case the self-reanimating chaos is observed. The irregular motion can be simulated numerically by imposing an extra noise on the coordinates of the point at which the reanimation occurs. This special point in the phase space will be described in Sec. III.

The paper is organized as follows. In Sec. II the scheme of experimental setup is given together with a qualitative description of the bouncing-ball model. The map used in numerical simulations is introduced in Sec. III, where the computer simulations are compared with the experimental results. Finally, Sec. IV summarizes our considerations; in particular, it contains a discussion of a class of maps, in which this kind of motion could occur.

II. EXPERIMENT

We consider below the bouncing-ball model known also as the jumping particle model.[3] The model (see Fig. 1) consists of a particle (e.g., a steel sphere) bouncing on a vibrating, horizontal surface (e.g., slightly concave glass lens fixed to the membrane of a loudspeaker). The loudspeaker is driven by a sinusoidal voltage of precisely controlled amplitude. The frequency of the vibration is in the range from 10 to 10^2 Hz. To simplify notation we shall often use in the following a dimensionless variable $\theta=2\pi\nu_0 t$, where t is the real time. The sounds of collisions between the ball and the surface are detected by a microphone. After a selective amplification the collision signals are shaped into identical pulses. Because of technical limitations the pulse-shaping procedure works properly for sufficiently loud collision sounds. Thus collisions which produce too weak sounds (following very low jumps) are not monitored by the detection circuit.[4]

Pulses produced by the collision detection system are processed by either analog or digital electronics. In the analog method, an oscilloscope is used to record the collision sequences within the collision phase-jump duration $(\tilde{\theta}_i,\tau_i)$ space. $\tilde{\theta}=\theta \pmod{2\pi}$ and $\tau_i=\theta_{i+1}-\theta_i$. The X

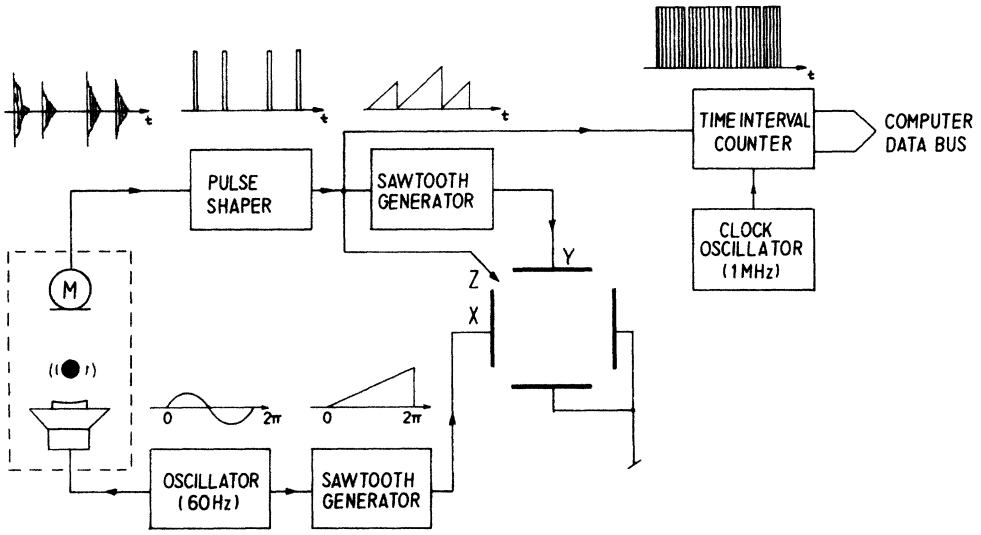

FIG. 1. Experimental setup.

input is controlled by a sawtooth voltage synchronized by the main sinusoidal signal (driving the loudspeaker). Consequently, the X position of the beam is always proportional to the phase θ of the surface motion. To make the Y position of the beam proportional to the jump duration τ_i, the Y input is controlled by applying a linearly increasing voltage reset by collision pulses. Before the linear generator is reset, the collision pulse reaches the beam intensity Z input of the oscilloscope. Thus the ith collision produces a bright dot on the screen: Its X and Y coordinates are proportional to $\bar{\theta}_i$ and τ_i, respectively.

In addition to the analog method, the sequence of collisions can be recorded digitally.[6] To convert τ_i into a digital form, a 1-MHz counter triggered and reset by successive collision pulses was used. Results of the consecutive counts were transferred (in the binary form) to a buffer memory and stored on a hard disk.

As described in our previous papers,[3] the ball can be put into a whole variety of stationary sequences as "modes." The simplest of the modes, denoted by $M^{(\alpha)}$, $\alpha=1,2,3,\ldots$, consists of equidistant-in-θ jumps between every α periods of the surface displacement function

$$h_S(\theta)=-H\cos(\theta)\ . \tag{1}$$

The $M^{(\alpha)}$ modes are stable in finite intervals $(H_0^{(\alpha)},H_1^{(\alpha)})$ of the surface vibration amplitude. $H_0^{(\alpha)}$ here denotes the threshold value below which the $M^{(\alpha)}$ mode cannot be sustained, since the momentum transfers from the vibrating surface are too small in order to compensate for the losses of the kinetic energy of the ball. On the other hand, the $M^{(\alpha)}$ modes lose their stability at the upper limits $H_1^{(\alpha)}$, giving rise to their period-doubled versions $M^{(\alpha,2)}$. In practice, up to 3 of such period doublings can be observed along the bifurcation tree of each $M^{(\alpha)}$ mode. In general, long period modes are stable at shorter H intervals occurring at larger values of the surface vibration amplitude H. The upper and lower boundary intervals are given approximately[3] by

$$H_0^{(\alpha)}\sim 2\pi(1-K)\alpha\ , \tag{2a}$$

$$H_1^{(\alpha)}\sim 2[(1+K)^2+(1-K)^2\pi^2\alpha^2]^{1/2}\ . \tag{2b}$$

The physical meaning of the constant K is explained in Sec. III. Typically, for steel spheres of diameter 3 mm, $K=0.86$. It seems worth emphasizing that due to the two-dimensional nature of the system, the $M^{(\alpha)}$ modes can coexist in the phase space.

Above the period-doubling cascade of the $M^{(1)}$ mode, one observes chaotic sequences of jumps. It is the main aim of the present paper to throw some light on these sequences. However, to understand their unusual features, one must first learn about still another mode, which to our knowledge has never been discussed. This mode denoted below by $M^{(0)}$ evolves in a natural way from the "ground state" of the model at which the ball lies still on the motionless surface. As the surface begins to oscillate, the ball remains in a continuous contact with it. In contrast to all other modes of the ball motion, this mode is mute. We denote it by $M_0^{(0)}$.

About a threshold value $H_1^{(0)}$ of the surface vibration amplitude, a chirping sound is heard. Figure 2(a) presents its oscilloscope image as monitored by a microphone after high-pass filtering. The sound consists of convergent sequences of strongly damped, high-frequency transients. The sequences appear at each period of the surface vibration and, strictly speaking, stand for the periodic motions for the system. The strongly damped, high-frequency transients correspond to the shrill sounds produced by the ball-surface collisions. Each convergent sequence of such sounds corresponds to a sequence of decaying jumps. (A similar convergent sequence of decaying jumps is observed when a ping-pong ball is dropped on the table.) It seems worth emphasizing that the audible sequences of decaying jumps are separated by mute intervals during which the ball moves in a continuous contact with the surface. This mode of the ball motion we denote as $M_1^{(0)}$.

As H increases, the chirping sound becomes louder; the convergent sequences of jumps become longer. When H exceeds the next threshold value $M_2^{(0)}$, the audibile periodicity of the chirping mode $M_1^{(0)}$ breaks down. Oscilloscope images, see Fig. 2(b), reveal that this is indeed true. The sequence of jumps becomes irregular, some of the jumps become higher, and one observes sometimes that the irregular sequence suddenly becomes periodic. This periodic motion is easily identified as either the $M^{(1)}$ mode or its period-doubled version $M^{(1,2)}$, depending on the value of H at which this transition took place. If H exceeds the limit $H_\infty^{(2)}$ of the period-doubling cascade of the $M^{(2)}$ mode, then no such effect is observed and the irregular sequence of jumps seems to be endless. Figure 3(a) presents a typical portrait of such a sequence recorded with the analog method within the $(\tilde{\theta}_i, \tau_i)$ space. Let us recall that the collision detection system we used could record neither too low jumps nor the whole intervals, if any, at which the ball was staying in continuous contact with the vibrating surface.

The experiments performed allow us to formulate the following scenario which shows how the motion of the ball evolves from its ground state as the surface vibration amplitude H slowly increases.

(i) $H \in (0, H_1^{(0)})$—the ball stays in the mute $M_0^{(0)}$ mode, i.e., it moves in continuous contact with the vibrating surface.

(ii) $H \in (H_1^{(0)}, H_2^{(0)})$—the chirping $M_1^{(0)}$ mode is heard.

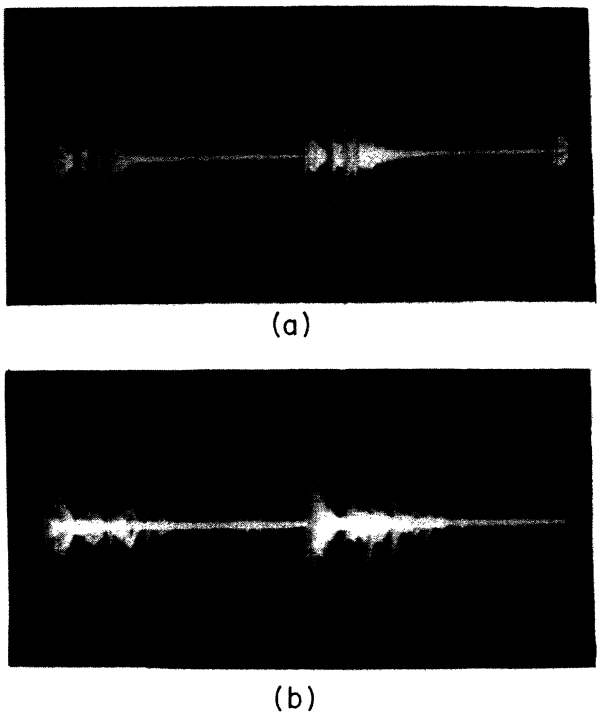

FIG. 2. High-frequency sound portraits of the $M^{(0)}$ mode at $\nu_0 = 13$ Hz. Exposure time covered about six periods of the surface vibration. (a) $M_1^{(0)}$ regular mode, $H \in (H_1^{(0)}, H_2^{(0)})$; (b) irregular mode observed above $H_2^{(0)}$.

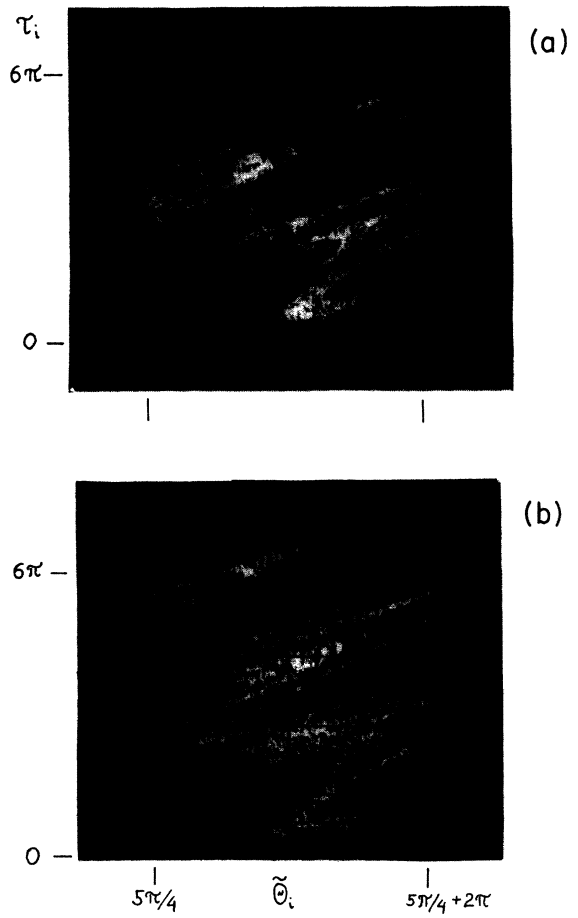

FIG. 3. $(\tilde{\theta}_i, \tau_i)$ space portrait of the chaotic C mode recorded in the system above the period-doubling cascade of the $M^{(2)}$ mode. $K = 0.86$ and (a) $\lambda = 5.17$; (b) $\lambda = 5.24$. K and λ are determined according to the fitting procedure described in Ref. 3.

At each period of the surface vibration the ball loses its continuous contact with the surface, and next executes a convergent sequence of decaying jumps and comes to the continuous contact again.

(iii) $H > H_2^{(0)}$—the chirping mode becomes unstable, it losses the periodicity, and through an irregular sequence of jumps it turns into the periodic $M^{(1)}$ mode.

(iv) $H \in (H_0^{(1)}, H_\infty^{(1)})$—the $M^{(1)}$ mode evolves through its period-doubling cascade.

(v) $H > H_\infty^{(1)}$—an irregular sequence of jumps is observed.

Details of the above scenario, especially points (iii), (iv), and (v) depend on experimental factors. Carrying on experiments in a setup based on a loudspeaker, one must make sure that its magnetic field does not perturb the steel-ball motion. If, for instance, the collision surface is placed too close to the loudspeaker's magnet, the effective field will not be homogeneous, which may lead to a qualitative change of the character of the $M_1^{(0)}$ mode. In general, in spite of its apparent triviality, the chirping model is a subtle phenomenon, much more susceptible to the external perturbations than the $\alpha 2\pi$-periodic $M^{(\alpha)}$ modes $(\alpha = 1, 2, 3, \ldots)$.

III. FORMAL DESCRIPTION OF THE MODEL AND NUMERICAL SIMULATIONS OF THE $M^{(0)}$ MODE

As was shown in our previous papers,[3] the $M^{(1)}$, $M^{(2)}$, and $M^{(3)}$ modes are well described by point attractors of the Zaslavski mapping

$$\vartheta_{i+1}=K\vartheta_i+\lambda\sin(\theta_{i+1}) , \tag{3a}$$

$$\theta_{i+1}=\theta_i+\vartheta_i . \tag{3b}$$

The attractors located in the $(\tilde{\theta}_i,\vartheta_i)$ space are

$$\vartheta^{(\alpha)}=\alpha 2\pi, \quad \alpha=1,2,3 , \tag{4a}$$

$$\theta^{(\alpha)}=\pi-\varepsilon^{(\alpha)}(\lambda) , \tag{4b}$$

where

$$\varepsilon^{(\alpha)}(\lambda)=\arcsin[(1-K)\alpha 2\pi\lambda^{-1}] . \tag{5}$$

The point attractor corresponding to $\alpha=0$ lies at $\vartheta^{(0)}=0$ and $\tilde{\theta}^{(0)}=0$. Hence it does not describe the $M^{(0)}$ mode at which the ball moving with the vibrating surface draws, in the $(\tilde{\theta},\vartheta)$ space, a sine-shaped line. To describe this kind of motion one must consider in more detail the dynamics of the system.

Let the horizontal collision surface oscillate vertically along the up-directed h axis [see Eq. (1)]. Let t_i be the time at which the ball leaves the surface beginning its ith jump with the initial velocity w_i measured in the laboratory reference frame. As it is shown in Ref. 5 the equations of motion of the bouncing ball (i.e., the relations between successive t_i and w_i) can be written as

$$w_{i+1}=K(gT_i-w_i)+(1+K)H\omega_0\sin(\omega_0 t_i) , \tag{6a}$$

$$t_{i+1}=t_i+T_i , \tag{6b}$$

$$-\tfrac{1}{2}gT_i^2+w_iT_i-H\cos(\omega_0 t_i)=-H\cos[\omega_0(t_i+T_i)] , \tag{6c}$$

where $T_i=t_{i+1}-t_i$ denotes the time length of the ith jump, $\omega_0=2\pi\nu_0$, and g is the gravitational acceleration. By putting

$$\theta_i=\omega_0 t_i, \quad \tau_i=\omega_0 T_i . \tag{7a}$$

$$\vartheta_i=2\omega_0 w_i g^{-1} , \tag{7b}$$

$$\lambda=2(1+K)H\omega_0^2 g^{-1} , \tag{7c}$$

Eqs. (6), are transformed into the dimensionless form

$$\vartheta_{i+1}=K(2\tau_i-\vartheta_i)+\lambda\sin(\theta_{i+1}) , \tag{8a}$$

$$\theta_{i+1}=\theta_i+\tau_i , \tag{8b}$$

$$-\tau_i^2+\vartheta_i\tau_i-[\lambda/(1+K)]\cos(\theta_i)=-[\lambda/(1+K)]\cos(\theta_i+\tau_i) , \tag{8c}$$

where K denotes the fraction of the ball velocity which survives a collision. Clearly, at $K=1$, the system becomes conservative. In dimensionless variables, the surface vibrates with a unit angular frequency and amplitude equal to $\lambda(K+1)^{-1}$. One can see that for the periodic $M^{(\alpha)}$ modes, Eq. (8c) is reduced to a simple equality $\tau_i=\vartheta_i$ and the whole map (8) takes the form of the Zaslavski map (3). In terms of this map, $M^{(\alpha)}$ modes are periodic both in time θ (the period is $\alpha 2\pi$) and in the iteration index i (the period is α), while in the $M_0^{(0)}$ mode the ball moves in continuous contact with the surface. Since the velocity ϑ^S of the latter changes with θ as

$$\vartheta^S=\lambda(1+K)^{-1}\sin(\theta) , \tag{9}$$

the variable values from the set $\{\theta_i,\ \vartheta_i=\vartheta^S(\theta_i),\ \tau_i=0\}$ should satisfy Eqs. (8). It is easy to prove that this is indeed the case. Let us notice, however, that for such values of θ_i, ϑ_i, and τ_i, iterations of the map (8) do not push forward the θ variable, while in reality it proceeds in a natural way (as the time flows).

Stability of the $M_0^{(0)}$ mode can be conveniently analyzed within the reference frame established by the vibrating surface. In this noninertial frame the ball is seen moving in the gravitational field, the acceleration constant g_S changes with θ as

$$g_S(\theta)=-2-\lambda(1+K)^{-1}\cos(\theta) . \tag{10}$$

For $0<\lambda<\lambda_1^{(0)}$, where

$$\lambda_1^{(0)}=2(1+K) , \tag{11a}$$

$$[-\lambda/(1+K)]\cos(\theta_1^{(0)})\geq 2 , \tag{11b}$$

the acceleration is always negative, i.e., the ball may safely lie on the surface for all θ. Thus the $M^{(0)}$ mode is stable up to $\lambda_1^{(0)}$. If λ exceeds $\lambda_1^{(0)}$, the ball may lie on the surface only for that part of the vibration period where $g_S(\theta)<0$.

Let

$$\theta_1^{(0)}(\lambda)=\arccos[-2(1+K)\lambda^{-1}] \tag{12}$$

denote those values of θ for which the ball leaves the surface due to the change of the sign of $g_S(\theta)$. In the laboratory frame we see that the ball begins to jump vertically with the velocity

$$\vartheta_i^{(0)}(\lambda)=\lambda(1+K)^{-1}\sin(\theta_1^{(0)}) . \tag{13}$$

The θ length of the first jump τ_1 can be found from Eq. (8c), while the next collision time $\theta_2^{(0)}$ can be found from Eq. (8b), and the velocity $\vartheta_2^{(0)}$ with which the ball starts the second jump can be found from Eq. (8a). Thus iterations of map (8) yields consecutive values of three variables θ_i, ϑ_i, and τ_i.

Notice that numerical iterations of map (8) are not as simple as those of map (3). Namely, Eq. (8c) from which θ lengths τ_i of consecutive jumps are determined must be solved by a separate procedure at each iteration. In practice we used the standard procedures (Newton algorithm and/or bisection method). For both methods the accuracy $\Delta\tau$ with which τ_i are determined must be finite and not less than the computer precision. This is equivalent to the presence of noise in the simulated system.

Using the procedure described above, we studied systematically the evolution of the $M^{(0)}$ mode. The results are shown in Fig. 4, where values of the phase $\tilde{\theta}^{(0)}$ at

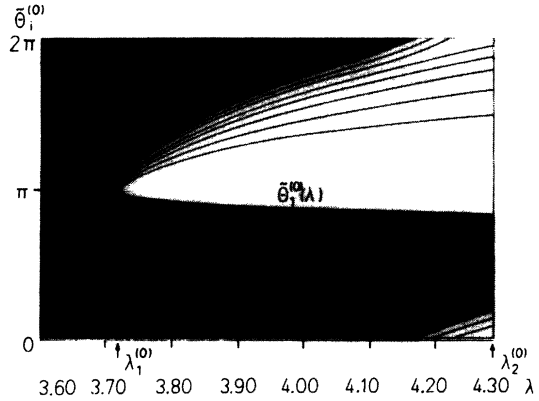

FIG. 4. Numerically determined evolution of the $M_1^{(0)}$ mode vs λ. Phases $\tilde{\theta}_i$ at which the ball collides with the surface are plotted in black. In the region filled in grey the collisions occur too close to each other to be separated. Phases at which the ball stays in a continuous contact with the collision surface are filled in black.

which the ball stays in contact with the collision surface are plotted versus λ. Below $\lambda_1^{(0)}$ the diagram is filled in black, which corresponds to the mute $M_0^{(0)}$ mode at which the ball moves throughout the whole (02π) interval, remaining in contact with the collision surface.

At $\lambda_1^{(0)}$, the $M_0^{(0)}$ mode loses its stability, turning into the $M_1^{(0)}$ mode. This is seen in Fig. 4 as a gap opening in the (02π) interval. Its lower border $\tilde{\theta}_1^{(0)}(\lambda)$ corresponds to the phase at which the ball loses its continuous contact with the collision surface. Phases $\tilde{\theta}_i^{(0)}$ at which the ball collides with the surface in the decaying sequence of jumps are seen to converge to the upper border of the gap $\tilde{\theta}_\infty^{(0)}(\lambda)$. In contrast to the lower border $\tilde{\theta}_1^{(0)}(\lambda)$ which can be determined analytically, see Eq. (12), the upper $\tilde{\theta}_\infty^{(0)}(\lambda)$ border must be estimated numerically. In Fig. 4 the latter was calculated by setting a lower limit $\tau_{\min}$ to the jump lengths τ_i. Below $\tau_{\min}$, the ball comes into continuous contact with the collision surface. Such a procedure cuts the infinite (but convergent) sequence of jumps above the number $N(\Delta\tau,\lambda)$. Of course $N\to\infty$ as $\Delta\tau\to 0$. ($\tau_{\min}$ is greater than the precision-of-zeros finding method $\Delta\tau$).

The $M_1^{(0)}$ mode is θ periodic, its θ period equals 2π. However, in contrast to the $M^{(1)}, M^{(2)}, \ldots$ modes, it is not i periodic.

The $(\tilde{\theta}_1^{(0)}(\lambda), \tilde{\theta}_\infty^{(0)}(\lambda))$ gap widens as λ increases. At $\lambda_2^{(0)}$ its width becomes equal to 2π. Thus the end of the first sequence of jumps meets the beginning of the next one. The $M_1^{(0)}$ mode loses its stability.

Further evolution of the $M^{(0)}$ mode is a subtle question. Three possibilities must be taken into account.

(i) The sequences of jumps are both θ and i periodic.

(ii) The sequences of jumps are θ periodic but i infinite (the intervals of continuous contacts between the ball and the surface would occur periodically in θ).

(iii) The sequences of jumps initiated at $\tilde{\theta}_1^{(0)}(\lambda)$ exist as transients leading to one of the $M^{(\alpha)}$, $\alpha>1$ modes or their bifurcated versions.

A general analysis of the problem needs extensive numerical studies. In this paper we limit the analysis to the $K=0.86$, $\lambda\geq\lambda_\infty^{(2)}$ case, which has been studied experimentally. It seems that option (iii) can be excluded here since above $\lambda_\infty^{(2)}$ both the $M^{(1)}$ and $M^{(2)}$ modes lose their periodicity. To find out which of the two remaining options is more probable, we iterated numerically map (8), starting from the $(\theta_1^{(0)},\vartheta_1^{(0)})$ point given by Eqs. (12) and (13). Calculations prove that after a finite number of iterations the sequence of τ_i starts to converge monotonically. Thus, if one sets a lower limit $\tau_{\min}$ to the values of τ_i, the iteration procedure will be stopped and the ball will stay in continuous contact with the collision surface. The trajectory calculated this way starts from and ends on the sine-shaped line indicating the motion of the collision surface. This result suggests that option (ii) is plausible. To check the sensitivity of the trajectory on initial conditions we performed the calculations starting from slightly different initial points $(\theta_1^{(0)}+\Delta,\vartheta_1^{(0)})$. As seen from Fig. 5, where the calculated trajectories are plotted, their i length changes strongly with the initial condition. It should be noted that in the real experiments the intrinsic noise is unavoidable. To simulate such conditions we performed long iteration runs in which whenever τ_i became shorter than $\tau_{\min}$, the iteration procedure was interrupted and restarted from a point chosen randomly from a close neighborhood of $(\theta_1^{(0)},\vartheta_1^{(0)})$. Figure 6(b) shows the results of such numerical runs performed for $K=0.86$

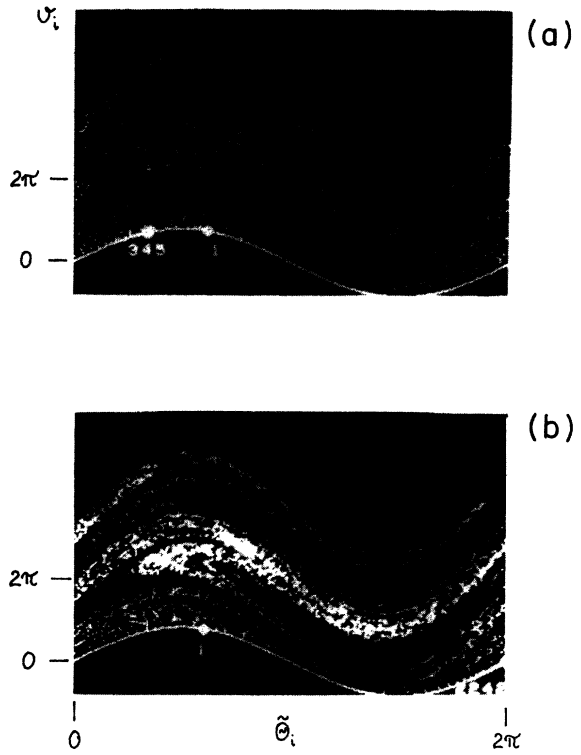

FIG. 5. Sensititivity on the initial conditions represented in the $(\tilde{\theta}_i,\vartheta_i)$ plane for $K=0.86$, $\lambda=4.93$. The initial point is $(\tilde{\theta}_1,\vartheta_1)=(\tilde{\theta}_1^{(0)}+\Delta,\vartheta_1^{(0)})$. (a) $\Delta=5\times10^{-3}$; (b) $\Delta=10^{-3}$. The initial ($i=1$) and final points ($i=345$ and 2242) of the trajectories are indicated in the plot with squares.

and $\lambda=5.03$. The calculated sequences of jumps are presented in the figure within the τ_{i+1} (τ_i) graph. In contrast to the experimental graphs [Fig. 6(a)] the low region is well visible here. The $(0,\tau_1^{(0)})$ point corresponds in the graph to the situation when the ball, after an interval of continuous contact with the surface, executes its first jump. The trajectory injected from the point into the (τ_{i+1},τ_i) space draws a complicated, strange-attractorlike figure and sinks into the (0,0) point corresponding to the continuous ball-surface contact.

As seen in Fig. 6(b), the return path is located within a thin horn connecting the bulk of the trajectory with the (0,0) point. In Fig. 7, where a similar trajectory is presented within the $(\tau_i,\tilde{\theta}_i)$ space, the return path is seen as a "band" tangent to the $\tilde{\theta}$ axis. A comparison of Fig. 7 with Fig. 3 convinces us that the map (8) well describes the bouncing-ball model in its experimental realization. The return paths are not reproduced by other maps.

To estimate the fractal dimension of attractors of the type shown in Fig. 6(b), we analyze[6] one of them ($K=0.86$, $\lambda=4.95$) with the Grassberger-Proccacia correlation integral method[7] obtaining $\nu_{\text{corr}}=1.37\pm0.11$. The multidimensional spectrum of the Lyapunov exponents[8] has been also analyzed giving $(\Lambda_1,\Lambda_1+\Lambda_2)=(+0.48,-0.37)$. The $(+,-)$ pattern of the Lyapunov exponents spectrum indicates the high sensitivity of the trajectory on external perturbations. The Lyapunov dimension $\nu_\Lambda=1+\Lambda_1/|\Lambda_2|=1.56$.

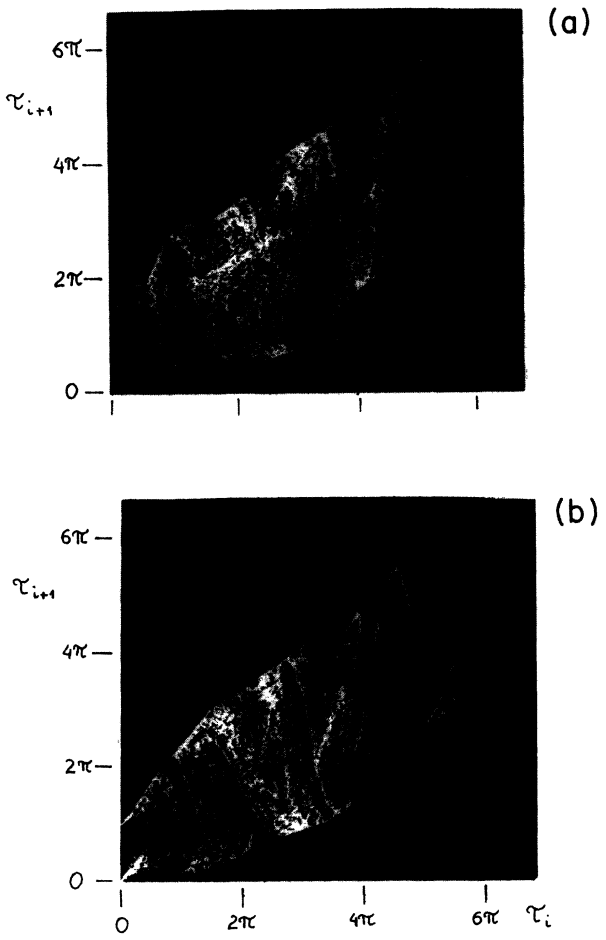

FIG. 6. τ_{i+1} (τ_i) portrait of the C mode. $K=0.86$ and (a) experimental, $\lambda=5.14$; (b) numerical, $\lambda=5.03$. The K and λ values specified for the experimental plot were determined according to the fitting procedure described in Ref. 3.

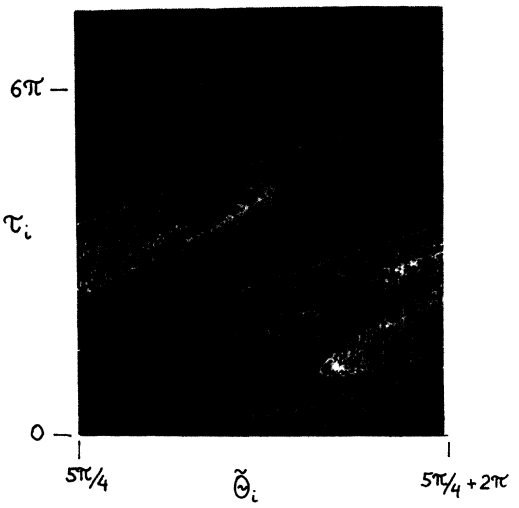

FIG. 7. τ_i $(\tilde{\theta}_i)$ portrait of the C mode calculated numerically for $K=0.86$ and $\lambda=5.17$.

IV. DISCUSSION

It is clear that the effect of self-reanimation in the bouncing-ball system is conditioned by the existence of the trivial mode, in which the ball remains continuously in the contact with the vibrating surface. If the amplitude of the vibrations is large enough for the ball to leave the surface, then the motion of the ball consists of periodically repeated series of decaying jumps and time intervals in which the ball is "stuck" to the surface. Obviously, the point of convergence (in the θ variable) of jump sequences increases with growing vibration amplitude. The self-reanimating chaos can appear when the series of jumps are not convergent, i.e., when the sum of all jump time intervals within one period of the surface vibration exceeds 2π. Although in the purely deterministic case this motion is periodic, the existence of noise and the sensitivity on the initial conditions destroy this periodicity. The period of the motion is the multiplicity of the period of the surface vibration.

A natural question that emerges from the above consideration is whether the self-reanimating chaos occurs in other physical systems or is it a particular feature of the bouncing-ball model. In other words, which properties of the map (8) are responsible for the occurrence of the self-reanimation effect? Since the Eq. (8c) is strongly nonlinear it can possess many different formal solutions. From the physical point of view we are interested only in the real situation when time intervals τ_i are non-negative. Because the ball cannot come through the surface, an additional requirement has to be imposed on Eq. (8c). Namely, the left-hand side of this equation cannot be less than the right-hand side. Thus, for ϑ_1 (θ_1), see Eq. (9), the following relation must be fulfilled:

$$-\tau^2+\tau[\lambda/(1+K)]\sin(\theta_1)-[\lambda/(1+K)]\cos(\theta_1) \geq -[\lambda/(1+K)]\cos(\theta_1+\tau)\ , \quad (14)$$

where $0<\tau<\tau_1$, with τ_1 being the time interval of the first jump. In the limit for $\tau\rightarrow 0_+$, the elementary algebra provides exactly the same relation as Eq. (11b) gave earlier from general considerations. In other words, Eq. (8c) for $\vartheta_1(\theta_1)=\vartheta^S(\theta_1)$ and $\theta_1\in[0,2\pi]$ [see also Eq. (12)] has one solution with $\tau_1=0$ and one solution with $\tau_1>0$. Because Eq. (8c) can possess more than one solution, the map (8) does not transform coordinates (θ_i,ϑ_i) into $(\theta_{i+1},\vartheta_{i+1})$ in a unique way. This seems to suggest that in order for a given two-dimensional map W to exhibit the self-reanimating chaos, it should satisfy the following assumptions.

(i) $W(\vartheta,\theta)=W(\vartheta,\theta+T)$, where $\theta=\theta(t)$ is monotonically increasing with time t and T is the period.

(ii) $\exists f\in C^1:\forall\theta\in[0,T]:W(f(\theta),\theta)=(f(\theta),\theta)$, i.e., a subset of fixed points of the map W forms a closed curve S^1 on the (ϑ,θ) plane.

(iii) $\exists\theta_1,\theta_2$ such that $0<\theta_1<\theta_2<T$: $\forall\theta\in[\theta_1,\theta_2]$: $W(f(\theta),\theta)\neq(f(\theta),\theta)$, what means together with (ii) that W loses its uniqueness in the $[\theta_1,\theta_2]$ subinterval.

(iv) $\exists\theta^*\notin[\theta_1,\theta_2];U=\{(\vartheta,\theta):\vartheta\neq f(\theta)\}:\forall(\vartheta_0,\theta_0)\in U$: $W^{(n)}(\vartheta_0,\theta_0)\rightarrow(f(\theta^*),\theta^*)$ as $n\rightarrow+\infty$.

It is easy to see that the dissipative Zaslavski map fulfills neither condition (ii) nor (iii), and therefore it cannot describe the self-reanimating chaos (this also concerns the case of the map discussed in Refs. 9 and 10).

Because the behavior of the bouncing-ball system is strongly dependent on the parameter values λ and K, it is an interesting problem if there are any particular values of these parameters for which the ball cannot "stick" to the surface, or equivalently, is the condition (iv) always fulfilled. Let us notice that assumption (iii) is valid for the map (8) only for $\lambda>\lambda_1^{(0)}$, see Eq. (11a) and Fig. 4. If the condition (iv) is not satisfied then instead of the self-reanimating chaos one should observe a "normal" behavior with the strange attractor. The numerical experiments, however, show that assumption (iv) is always fulfilled in the map (8). (See also Ref. 11.) Thus only simple periodic orbits in their based or bifurcated versions and/or the self-reanimating chaos (coexisting with them for $\lambda>\lambda_1^{(0)}$) are observed.

ACKNOWLEDGMENTS

We thank Professor J. Małecki and Professor J. Stankowski for stimulating discussion and Dr. W. Jeżewski and Dr. B. Sczaniecki for useful remarks. This work was partially supported by the Polish Academy of Sciences under Project No. CPBP-01-12.

*Present address: Institute of Physics, Higher Educational School, PL-30-084 Krakow, Poland.

[1]G. M. Zaslavski, *Statistical Irreversibility in Nonlinear Systems* (in Russian) (Nauka, Moscow, 1970); Phys. Lett. **69A**, 145 (1978).

[2]A. J. Lichtenberg and M. A. Lieberman, *Regular and Stochastic Motion* (Springer-Verlag, New York, 1983); A. J. Lichtenberg, M. A. Lieberman, and R. H. Cohen, Physica D **1**, 291 (1980); J. Guckenheimer and P. J. Holmes, J. Sound Vib. **84**, 173 (1982); B. V. Chirikov, Phys. Rep. **52**, 263 (1979).

[3]P. Pierański, J. Phys. (Paris) **44**, 573 (1983); P. Pierański, Z. J. Kowalik, and M. Franaszek, *ibid.* **46**, 681 (1985).

[4]N. B. Tuffillaro, T. M. Mello, Y. M. Choi and A. M. Albano, J. Phys. (Paris) **47**, 1477 (1986); T. M. Mello and N. B. Tufillaro, Am. J. Phys. **55**, 316 (1987).

[5]C. Grebogi, E. Ott, and J. A. York, Physica D **7**, 181 (1983); H. Kantz and P. Grassberger, *ibid.* **17**, 75 (1985).

[6]M. Franaszek and Z. J. Kowalik, Phys. Rev. A **33**, 3508 (1986).

[7]P. Grassberger and I. Procaccia, Physica D **4**, 189 (1983).

[8]I. Shimada and T. Nagashima, Prog. Theor. Phys. **61**, 1605 (1979).

[9]R. V. Jensen and C. R. Oberman, Physica D **4**, 183 (1982): K. Y. Tsang and M. A. Lieberman, Phys. Lett. **103A**, 175 (1984).

[10]R. M. Everson, Physica D **19**, 355 (1986).

[11]S. Celaschi and R. L. Zimmerman, Phys. Lett. **120A**, 447 (1987).

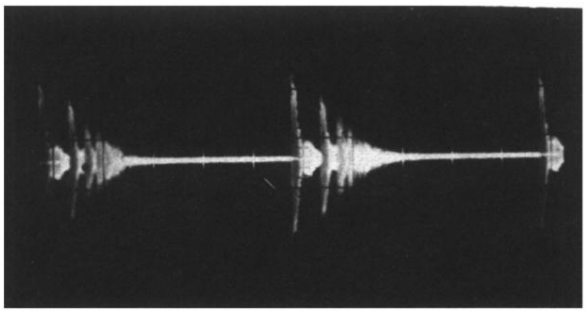

(a)

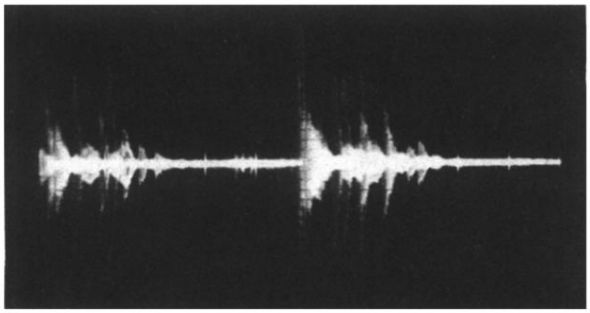

(b)

FIG. 2. High-frequency sound portraits of the $M^{(0)}$ mode at $\nu_0 = 13$ Hz. Exposure time covered about six periods of the surface vibration. (a) $M_1^{(0)}$ regular mode, $H \in (H_1^{(0)}, H_2^{(0)})$; (b) irregular mode observed above $H_2^{(0)}$.

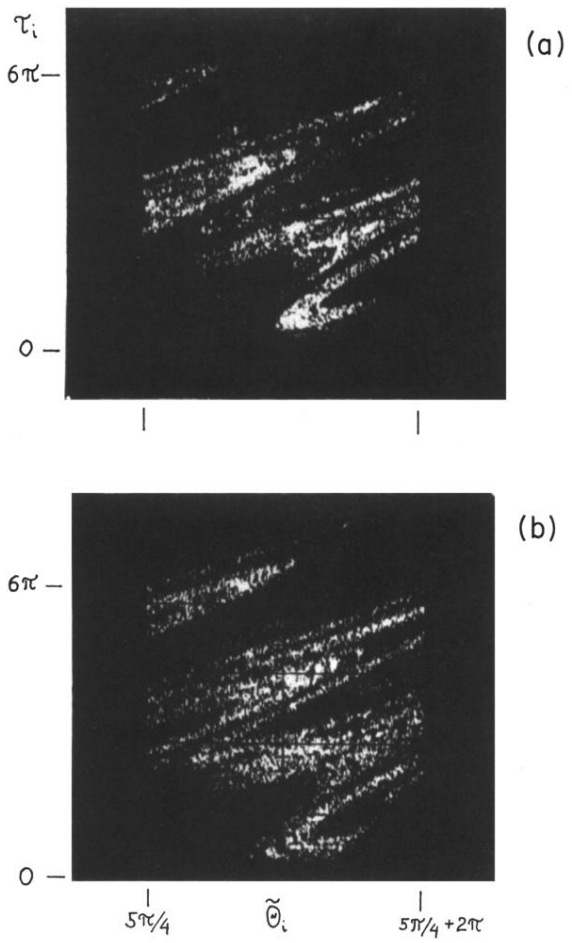

FIG. 3. $(\tilde{\theta}_i, \tau_i)$ space portrait of the chaotic C mode recorded in the system above the period-doubling cascade of the $M^{(2)}$ mode. $K=0.86$ and (a) $\lambda=5.17$; (b) $\lambda=5.24$. K and λ are determined according to the fitting procedure described in Ref. 3.

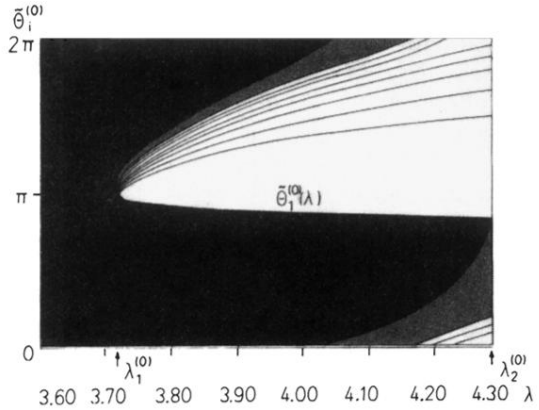

FIG. 4. Numerically determined evolution of the $M_1^{(0)}$ mode vs λ. Phases $\tilde{\theta}_i$ at which the ball collides with the surface are plotted in black. In the region filled in grey the collisions occur too close to each other to be separated. Phases at which the ball stays in a continuous contact with the collision surface are filled in black.

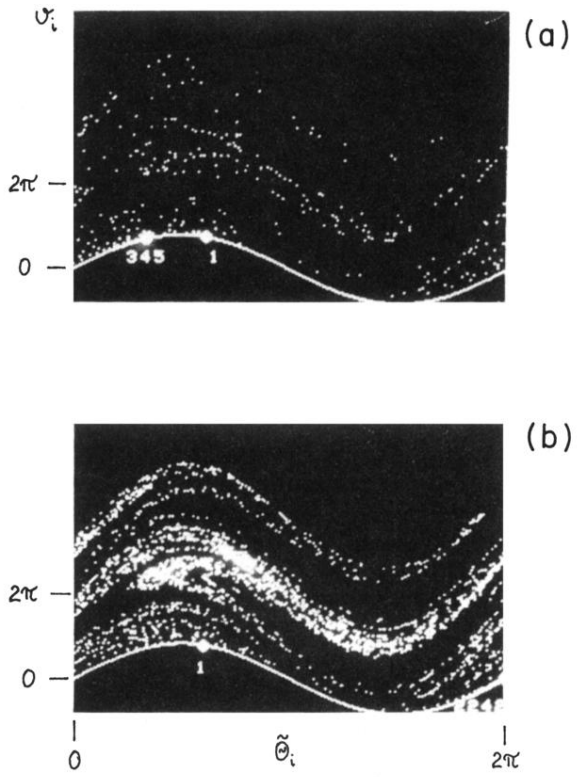

FIG. 5. Sensititivity on the initial conditions represented in the $(\tilde{\theta}_i, \vartheta_i)$ plane for $K=0.86$, $\lambda=4.93$. The initial point is $(\tilde{\theta}_1, \vartheta_1)=(\tilde{\theta}_1^{(0)}+\Delta, \vartheta_1^{(0)})$. (a) $\Delta=5\times10^{-3}$; (b) $\Delta=10^{-3}$. The initial ($i=1$) and final points ($i=345$ and 2242) of the trajectories are indicated in the plot with squares.

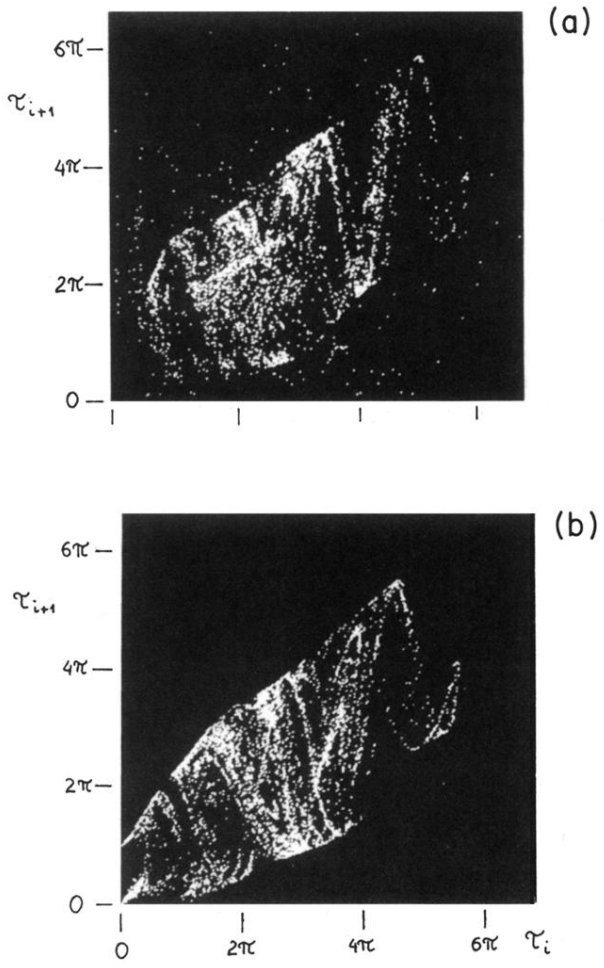

FIG. 6. $\tau_{i+1}(\tau_i)$ portrait of the C mode. $K=0.86$ and (a) experimental, $\lambda=5.14$; (b) numerical, $\lambda=5.03$. The K and λ values specified for the experimental plot were determined according to the fitting procedure described in Ref. 3.

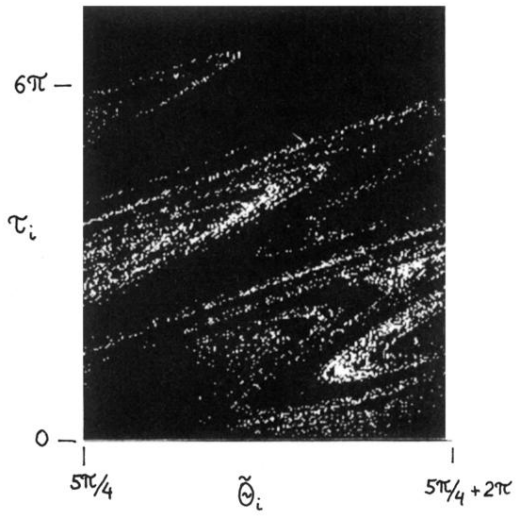

FIG. 7. τ_i $(\tilde{\theta}_i)$ portrait of the C mode calculated numerically for $K=0.86$ and $\lambda=5.17$.